Tunable-Delay Shunts for Paper Microfluidic Devices

Bhushan J. Toley, Brittney McKenzie, Tinny Liang, Josh Buser, Paul Yager, and Elain Fu

Department of Bioengineering
University of Washington
Seattle, WA 98195

Running Title: Delaying shunts for paper-based devices

Correspondence to:
Elain Fu
School of Chemical, Biological, and Environmental Engineering
Oregon State University
Email: elain.fu@oregonstate.edu

Supporting Information

I. Material Properties

The wicking rate of each material was determined by measuring the time required for a phenol red solution at pH 7.0, to wick 4 cm into 4.6 mm wide strips of the material. The absorption capacity of each material was determined by dipping one edge of a 1 cm x 1 cm piece of the material into a beaker of DI water, located on a balance, and measuring the decrease in water mass. The permeability and capillary pressure of each material were measured using a method developed in our lab, based on monitoring the flow rate of fluids through a material under a fixed pressure drop (manuscript in preparation). Preliminary measurements yielded the values listed in Table S1.

Table S1

	Absorption Capacity ($\mu l/cm^2$)	Wicking Rate (s/4 cm)	Thickness (mm)	Permeability (DI water) (10^{-13} m^2)	Capillary Pressure (DI water) (Pa)
Nitrocellulose FF80HP	10	80	0.09	7.6	13,000
Cellulose CFSP223000	83	70	0.87	37	3,000
Cellulose 320	350	28	2.7	120	2,100

The nominal cellulose shunt in this model had a 2.5-fold greater absorption capacity, a 0.5-fold greater fluidic resistance, and a 1.1-fold greater capillary force than the nitrocellulose channel. These model input parameters were consistent with the experimentally measured values for the permeability, capillary pressure, wicking rate, and absorption capacity of the nitrocellulose and cellulose (Table S1). For example, cellulose CFSP223000 was measured to have a greater absorption capacity and a smaller fluidic resistance (greater permeability) than the nitrocellulose.

There was also consistency in the case of the parameter of capillary force, which depends on the product of the capillary pressure and the cross-sectional area for wicking. Though the nitrocellulose was measured to have a greater capillary pressure than cellulose CFSP223000, the cross-sectional area of the cellulose CFSP223000 was significantly greater than that of the nitrocellulose (~870 μm thickness for cellulose compared to ~90 μm for nitrocellulose). Thus, these measurements are consistent with an input parameter of a 1.1-fold greater capillary force for the cellulose CFSP223000 compared to the nitrocellulose.

II. Protocol for the Demonstration of Shunt Compatibility with Biochemical Reagents

A murine antibody to *Plasmodium falciparum* histidine rich protein 2 (*Pf*HRP2) (*National Bioproducts Institute*, Pinetown, South Africa) was hand spotted at 1 mg/mL onto the detection region of a paper network composed of nitrocellulose. A second murine antibody to *Pf*HRP2 (*National Bioproducts Institute*, Pinetown, South Africa) conjugated to a gold nanoparticle (*BBInternational*, Cardiff, UK) served as a label. The conjugate at optical density 10 was combined with 1% BSA in TBS, 5% sucrose in water, 5% trehalose in water in volume ratios of 5:1:2:2 respectively. A 12 μl volume of the mixture was dried in a 4 mm x 5 mm glass fiber pad. To minimize nonspecific adsorption, the hand spotted paper network was soaked in a solution of 0.25% BSA, 0.25% PVP, 5% sucrose in phosphate buffered saline for 30 minutes then dried in a desiccator overnight. The sample consisted of 20 ng/mL of recombinant malaria protein *Pf*HRP2 (*CTK Biotech*, San Diego, CA) spiked into fetal bovine serum (*Invitrogen*, Carlsbad, CA). The signal amplification reagents were a set of solutions for gold enhancement (*Nanoprobes*, Yaphank, NY). The four solutions were mixed according to manufacturer instructions in a 1:1:1:1 ratio before application to the network.

III. Electrical Circuit Model of an Absorbent Pad-based Shunt on a Porous Channel

A length of dry porous material with a fluid source at one end may be represented by an electrical circuit as shown schematically in Fig. 1D. If fluid is introduced at one end of such a porous channel at time $t = 0$, consider a time, t, at which the fluid front has traveled a distance, $d(t)$, through the channel. Voltage, V, is analogous to the capillary force generated by the porous material and electrical ground is analogous to the fluid source. The electrical resistance, $R(t)$, is analogous to the fluidic resistance of the material and t is the time after the fluid source is introduced. As the fluid front progresses through the channel of porous material, the capillary force generated at the liquid-air-solid interface at the fluid front must pull fluid through a greater length of material. Thus, the fluidic resistance increases linearly with distance as the fluid front progresses though the material. Current, $i(t)$, generated in the electrical circuit is analogous to the flow rate of fluid through the porous material and can be calculated using Ohm's law.

$$i(t) = \frac{V}{R(t)} \tag{S1}$$

The circuit analogy can be extended for systems that include multiple porous materials. For the shunt system composed of a porous material main channel, in contact with a different porous material shunt, an analogous electrical circuit is shown in Fig. 1E. The system can be broken down into multiple pieces, each represented by a voltage and time-dependent resistance. The main channel is represented by three resistances in series – resistance from the portion of the channel upstream of the shunt, $R_{channel,U}$, the portion of the channel in contact with the shunt, $R_{channel,V}$, and the portion of the channel downstream of the shunt, $R_{channel,D}$. The shunt is represented by a resistance, R_{shunt}, in parallel with $R_{channel,V}$. The values of all resistances in this circuit depend on the location of the fluid front. The values of the voltages also depend on the location of the fluid front. A fully wetted section of the assembly has no ability to imbibe fluid

and is represented by a zero voltage, while any section of the assembly that has capacity for imbibition is represented by a non-zero voltage. The shunt generates a voltage V_{shunt}, and the main channel generates a voltage $V_{channel}$. The voltage generated by the main channel may be from the upstream portion, $V_{channel,U}$, from the portion in contact with the shunt, $V_{channel,V}$, or from the downstream portion, $V_{channel,D}$. The magnitudes of $V_{channel,U}$, $V_{channel,V}$, and $V_{channel,D}$ are equal, but the voltages are turned on at different times. Application of Kirchoff's voltage law to loops **ghjklmnog** and **ghjpqmnog**, and Kirchoff's current law to nodes **j** and **m** (Fig. 1E) yields the following relations that relate the parameters.

$$V_{channel,U} + V_{channel,V} + V_{channel,D} = i_1(t)R_{channel,U}(t) + i_2(t)R_{channel,V}(t) + i_4(t)R_{channel,D}(t) \quad \text{(S2)}$$

$$V_{channel,U} + V_{shunt} + V_{channel,D} = i_1(t)R_{channel,U}(t) + i_3(t)R_{shunt}(t) + i_4(t)R_{channel,D}(t) \quad \text{(S3)}$$

$$i_2(t) + i_3(t) = i_4(t) \quad \text{(S4)}$$

$$i_2(t) + i_3(t) = i_4(t) \quad \text{(S5)}$$

These equations can be solved simultaneously for the currents $i_1(t)$, $i_2(t)$, $i_3(t)$, and $i_4(t)$.

A step-by-step progression of fluid through the assembly of Fig. 1E and the equivalent electrical circuit at each stage is shown in Fig. S1. Consider that fluid is introduced into the nitrocellulose channel at one end of the assembly at $t = 0$. Before the fluid front reaches the shunt, the assembly can be represented by a circuit as shown in Fig. S1A. The distance traveled by the fluid front in this upstream portion of the nitrocellulose channel is $d_{channel,U}(t)$. The nitrocellulose channel upstream of the cellulose shunt is represented by a time-dependent resistance, $R_{channel,U}(t)$, and voltage, $V_{channel,U}$, and all other voltages and resistances are set to zero (Fig. S1A). This circuit is equivalent to the circuit for a standalone nitrocellulose channel (Fig. 1D). The following relations can be written:

$$d_{channel,U}(t) = C_{1,channel} \int_0^t i_1(t)\,dt \quad \text{(S6)}$$

$$R_{channel,U}(t) = C_{1,channel}\ C_{2,channel} \int_0^t i_1(t)\,dt \quad \text{(S7)}$$

Here $C_{1,channel}$ is inversely related to the absorption capacity of the nitrocellulose channel and $C_{2,channel}$ is a measure of the fluidic resistance and inversely proportional to the fluidic permeability of nitrocellulose. For a fixed volume of fluid wicked into the material (charge passed through the circuit), as the capacity increases, the distance traveled through the nitrocellulose channel decreases, assuming that there is no variation in the location of the fluid front along the thickness of the nitrocellulose. The fluidic resistance to wicking offered by the channel is proportional to the wet length of the channel.

After the fluid front enters the shunt region, it distributes into the cellulose shunt and the nitrocellulose channel under it. The cellulose shunt can be represented by voltage, V_{shunt}, and a time-dependent resistance, $R_{shunt}(t)$. The nitrocellulose under the cellulose can be represented by voltage, $V_{channel,S}$, and a time-dependent resistance, $R_{channel,S}(t)$ (Fig. S1B). The transfer of fluid from nitrocellulose to the cellulose is associated with a contact resistance, R_{con}. The upstream portion of nitrocellulose, which is fully wet, has a zero voltage and has reached maximum resistance, $R_{channel,U,max}$. Assuming that the fluid front reaches the cellulose shunt region at $t = t_s$, the following relations can be written:

$$d_{channel,S}(t) = C_{1,channel} \int_{t_s}^t i_2(t)\,dt \quad \text{(S8)}$$

$$R_{channel,S}(t) = C_{1,channel}\ C_{2,channel} \int_{t_s}^t i_2(t)\,dt \quad \text{(S9)}$$

$$d_{channel,D}(t) = C_{1,channel} \int_{t_s}^{t} i_4(t)\,dt \quad \text{(S10)}$$

$$R_{shunt}(t) = C_{1,shunt}\ C_{2,shunt} \int_{t_s}^{t} i_3(t)\,dt \quad \text{(S11)}$$

where $d_{channel,S}$ and d_{shunt} are the distances traversed by the fluid front in the nitrocellulose channel in contact with the cellulose shunt, and in the cellulose shunt, respectively. Under certain combinations of resistance and voltage values, this circuit produces negative currents in some branches. However, because the flow of fluid from a dry part of the paper device to a wet part is not possible, negative currents were interpreted as zero flow rate. In experiments performed with the system used in this study, the fluid front in the cellulose shunt traveled faster compared to the fluid front in the nitrocellulose channel (Fig. 4B). When the cellulose shunt becomes saturated with fluid, voltage V_{shunt} is set to zero and R_{shunt} reaches its maximum value $R_{shunt,max}$ (Fig. S1C). Finally, after the cellulose shunt and the nitrocellulose channel under the shunt are fully wet, fluid progresses into the downstream part of the nitrocellulose channel (Fig. S1D). $V_{channel,S}$ is set to zero, $R_{channel,S}$ reaches its maximum value, $R_{channel,S,max}$, and the downstream part of the channel is represented by voltage $V_{channel,D}$ and resistance $R_{channel,D}(t)$. If the fluid front exits the nitrocellulose channel under the cellulose shunt at $t = t_e$, the following relations can be written:

$$d_{channel,D}(t) = C_{1,channel}\ C_{2,channel} \int_{t_e}^{t} i_4(t)\,dt \quad \text{(S12)}$$

$$R_{channel,D}(t) = C_{1,channel}\ C_{2,channel} \int_{t_e}^{t} i_4(t)\,dt \quad \text{(S13)}$$

where $d_{channel,D}$ is the distance traveled by the fluid front in the downstream part of the nitrocellulose channel. The location of fluid fronts as a function of time can be derived by solving the electrical circuit equations (S2) through (S5) for currents. At each time iteration, the values of voltages and resistances are updated using the relevant relations from equations (S8) through (S13) for the current fluid front locations.

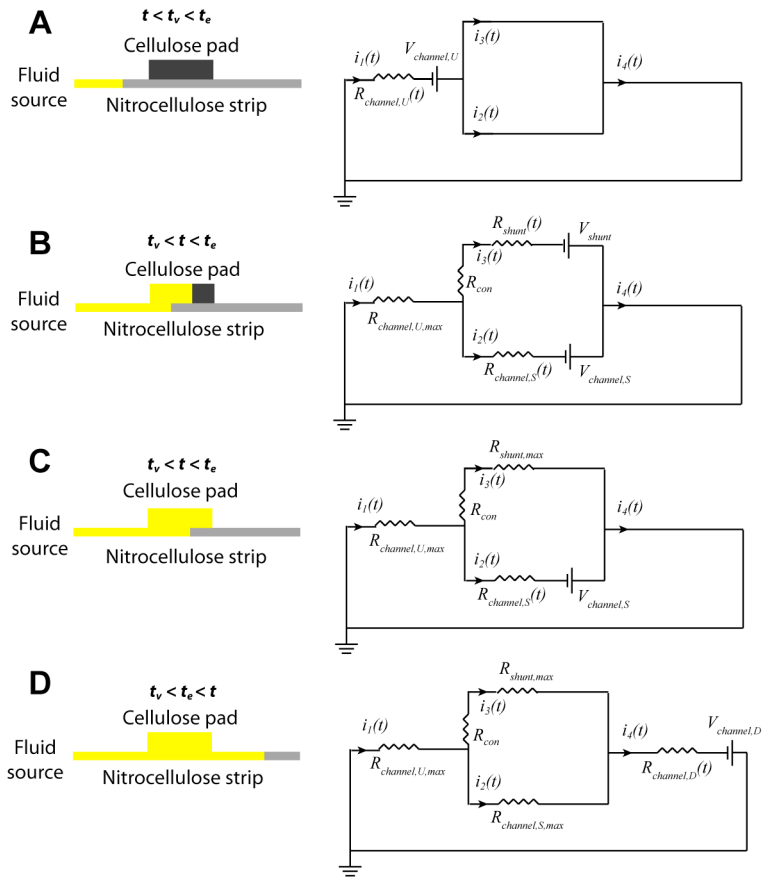

Figure S1. Electrical circuit representations of the assembly at different times depending on the location of the fluid front.

IV. Analytical Solution for Fluid Progress through a Porous Material using Ohm's Law

An analytical solution produces the linear relationship between distance traveled and the square root of time predicted by the Washburn equation. Equations (S1), (S6), and (S7) define the electrical equations associated with fluid flow through a porous channel. Substituting for $R(t)$ from equation (S7) into equation (S1):

$$i(t) = \frac{V}{C_1\ C_2 \int_0^t i(t)\,dt} \tag{S14}$$

$$\Rightarrow i(t) \int_0^t i(t)\,dt = \frac{V}{C_1\ C_2} \tag{S15}$$

In order to solve this equation analytically, the following mathematical substitution can be made:

$$y(t) = \int_0^t i(t)\,dt \tag{S16}$$

Rewriting equation (S15) using (S16) produces:

$$\frac{dy(t)}{dt} y(t) = \frac{V}{C_1 C_2} \tag{S17}$$

This equation can be integrated to obtain:

$$y(t) = \int_0^t i(t)\,dt = \sqrt{\frac{2V}{C_1 C_2}}\sqrt{t} \tag{S18}$$

Substituting this result into equation (S6) yields:

$$d(t) = \sqrt{\frac{2VC_1}{C_2}}\sqrt{t} \tag{S19}$$

This indicates that the distance traversed by the fluid front during wicking is proportional to the square root of time.

V. Effect of Spacer Thickness in the Folding Card Format

The effect of the thickness of the spacer in the folding card format on the delay was investigated. For a 15.2 mm long shunt (cellulose CFSP223000) on a porous channel (nitrocellulose FF80HP), a 10-mil thick spacer in the folding card produced a delay that was significantly lower than that produced by a 15.2 mm long shunt in the bench-top system (*, $P<0.05$; N=4; Fig. S2A). Decreasing the thickness of the spacer from 10 mil to 8 mil, and from 8 mil to 6 mil, significantly increased the delays (*, $P<0.05$; N=4). Further decreasing the spacer thickness to 4 mil did not change the delay significantly. Note that although varying the spacer thickness is expected to affect the contact resistance, an additional potential effect is to change the capillary pressure and permeability due to compression of the pores in the material.

The effect of varying the contact resistance, R_{con}, from its nominal value, $R_{con} = 0$ was explored in the model. The results showed that initially, small increases in contact resistance produced increases in the delay, but subsequent increases in contact resistance produced decreases in the delay (Fig. S2B).

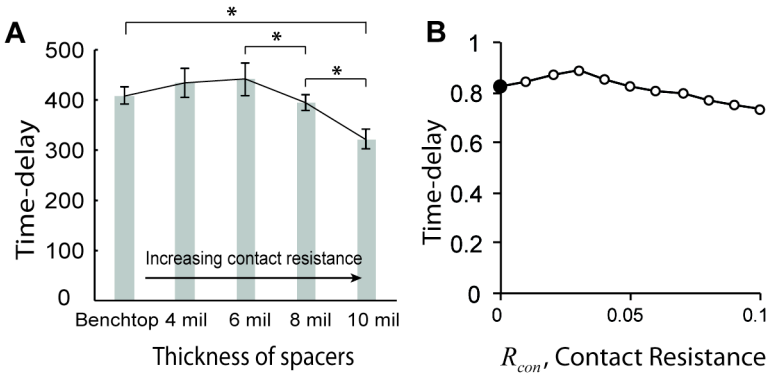

Figure S2. Effect of spacer thickness on delay in a folding card. **A**. Experimentally observed delays as a function of the thickness of spacers in the card. Initially increasing the thickness slightly increased the delay, but then further increasing the thickness, decreased the delay. **B**. Model predictions of time delay as a function of the contact resistance, R_{con}. The model predicted a similar trend to that observed in the experimental results. Increasing the contact resistance from zero (analogous to in the bench-top set-up) initially increased delays, but for further increasing the contact resistance decreased the delay.

VI. Tracking Fluid Fronts in a System of Cellulose and Nitrocellulose

Flow through a system of nitrocellulose (FF80HP) as the main channel and cellulose (CFSP223000) as the absorbent pad shunt was characterized. In order to simultaneously track the fluid fronts in both materials, a 30.5 mm cellulose pad in contact with a nitrocellulose strip oriented with the cellulose on top, and an identical assembly oriented with the cellulose on the bottom, were placed, along with a control of nitrocellulose strip only, in a folding card format (Fig. S3). Fluid was introduced simultaneously to both assemblies and the progress of the fluid fronts through the nitrocellulose strip under the cellulose pad (left-side strip; Fig. S3) and through the cellulose pad (right-strip; Fig. S3) was recorded. The fluid fronts in both strips traveled at an equal velocity upstream of the cellulose pad. After entering the shunt region, the fluid fronts slowed down, but the fluid front in the cellulose progressed faster downstream than the fluid front in the nitrocellulose.

The location of each fluid front was plotted against the square root of time (Fig. 4B). The control exhibited a linear behavior in accordance with the Washburn equation. In the shunt region, the fluid fronts decreased in velocity, as expected. However, the fluid front in the nitrocellulose (red line; Fig 4B) traveled more slowly than in the cellulose (green line; Fig, 4B). When the fluid front in the cellulose reached the end of the pad, the fluid front in nitrocellulose was lagging. After the cellulose pad saturated, the speed of the fluid front in the nitrocellulose increased and it traversed the remaining length of the pad rapidly. Downstream of the shunt region, the fluid front location in both strips coincided. The faster progress of fluid through the cellulose compared to the nitrocellulose in the region of the shunt is a result of the specific combination of capillary force and fluidic resistance of the cellulose *vs.* nitrocellulose materials. Cellulose offers a lower resistance to flow due to its larger average pore diameter. However, the

capillary pressure generated by a porous material is inversely proportional to the average pore diameter. The capillary force generated by the material is a product of the capillary pressure and the cross sectional area over which the pressure is exerted. For materials with a very large pore diameter, the capillary pressure, and therefore the capillary force generated may be too small to wick fluid. Cellulose CFSP223000 has the appropriate combination of capillary force and fluidic resistance for producing delays in nitrocellulose FF80HP channels because fluid is diverted into the cellulose when placed in contact with nitrocellulose.

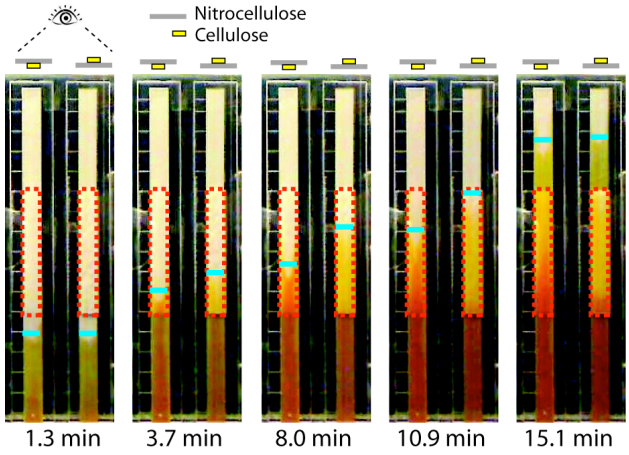

Figure S3. Time-lapse images showing a comparison of the locations of fluid fronts in the nitrocellulose (left strip) vs. cellulose (right strip) in an assembly at different times. The fluid front in the cellulose shunt traveled faster than in the nitrocellulose channel in contact with it.

VII. Additional Model Predictions of the Effect of Shunt Material

The electrical circuit model was used to predict the effect of material properties on the resulting delays. Manufacturers of porous materials typically provide values for two properties associated with the material – the absorption capacity and the wicking rate. Wicking rate, in turn, is dependent on two parameters – the capillary force generated by the material on a given fluid (V_{shunt}), and the resistance to flow ($C_{2,shunt}$, inversely related to the permeability) of the material to a given fluid. The effect of each parameter was investigated by perturbing one parameter at a

time from the nominal case. When the shunt resistance ($C_{2,shunt}$) is high, the delays are shortest (right extreme on x-axis; Fig. S4A). Under these conditions, inadequate flow into the shunt causes fluid to flow downstream of the shunt before the shunt material is fully wet. As the shunt material resistance decreases, the delays increase (Fig. S4A). At a certain value of shunt material resistance, the delay is maximized. As the shunt resistance is decreased further beyond this point, the delay decreases (left extreme on x-axis; Fig. S4A), as a result of rapid filling of the shunt, followed by flow downstream of the shunt. A similar trend exists for the effect of the capillary force (V_{shunt}) of the material on delays. At low capillary forces, the delays are the shortest (Fig. S4B) due to inadequate flow into the shunt and premature flow downstream of the shunt. As the capillary force increases, the delay increases and reaches the maximum at a certain capillary force (Fig. S4B). Further increase in the capillary force causes rapid fluid flow into the shunt and saturation of the shunt, followed by subsequent flow downstream in the channel, decreasing the delays (Fig. S4B).

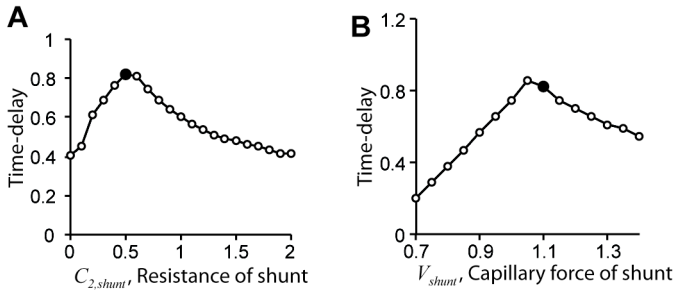

Figure S4. The effects of fluidic resistance (inversely related to permeability) and capillary force on delays as predicted by the electrical circuit model. **A**. There is a fluidic resistance ($C_{2,shunt}$) at which the delay is maximized (solid data point). **B**. Similarly, there is a capillary force (V_{shunt}) that maximizes the delay (solid data point).